Available online at www.sciencedirect.com
SCIENCE DIRECT®
Journal of Chromatography A, 989 (2003) 207–219
JOURNAL OF CHROMATOGRAPHY A
www.elsevier.com/locate/chroma

Influence of the particle porosity on chromatographic band profiles

Wojciech Piątkowski[a,b,c], Fabrice Gritti[a,b], Krzysztof Kaczmarski[c], Georges Guiochon[a,b,*]

[a]*Department of Chemistry, University of Tennessee, 552 Buehler Hall, Knoxville, TN 37996-1600, USA*
[b]*Division of Chemical and Analytical Sciences, Oak Ridge National Laboratory, Oak Ridge, TN, USA*
[c]*Faculty of Chemistry, Rzeszów University of Technology, W. Pola 2 Street, 35-959 Rzeszów, Poland*

Received 17 October 2002; received in revised form 19 December 2002; accepted 20 December 2002

Abstract

The mass transfer kinetics of butyl benzoate, eluted on a monolithic RPLC column with methanol–water (65:35, v/v) as the mobile phase was investigated, using the perturbation method to acquire isotherm data and the mobile phase velocity dependence of the height equivalent to a theoretical plate of perturbation peaks to acquire kinetics data. The equilibrium isotherm of butyl benzoate is accounted for by the liquid–solid extended multilayer BET isotherm model. The total porosity of the column varies much with the butyl benzoate concentration, influencing strongly the parameters of its mass transfer kinetics and the profiles of the breakthrough curves. Using all these parameters, the general rate model of chromatography predicts band profiles and Van Deemter curves that are in excellent agreement with experimental results provided the influence of concentration on the porosity is properly taken into account. This agreement confirms the validity of the models selected for the isotherm and for the mass transfer kinetics.

Keywords: Band profiles; Monolithic columns; Frontal analysis; Perturbation chromatography; Adsorption isotherms; Nonlinear peaks; Mathematic modelling; Porosity; Mass transfer; Kinetic studies; Stationary phases, LC

1. Introduction

Preparative liquid chromatography is more and more frequently used for the separation and purification of pharmaceutically and biologically active compounds. Chromatographic separations usually involve a complex mass transfer mechanism that strongly influences band broadening. Thus, in order to achieve an accurate prediction of these processes, the mass transport kinetics should be quantitatively described in addition to the equilibrium thermodynamics. A correct mathematical model of this kinetics is necessary for an accurate optimization of the design and operating parameters of novel separations for maximum productivity of the process. When the mass transport kinetics is slow, the general rate (GR) model is the most accurate tool for the prediction of band profiles. This model accounts well for all the contributions to band broadening: axial dispersion, external and internal mass transfer resistances and provides a reliable method of calculation of elution band profiles [1–4].

The solution of this model, however, involves the simultaneous calculation of concentration profiles in the column and within the particles, along the space and time coordinates. Solving this model requires

*Corresponding author. Tel.: +1-865-974-0733; fax: +1-865-974-2667.
E-mail address: guiochon@novell.chem.utk.edu (G. Guiochon).

0021-9673/03/$ – see front matter
doi:10.1016/S0021-9673(03)00003-7

complex and time consuming numerical techniques; typically the orthogonal collocation on fixed element method [5] is employed.

In separate reports [6,7], we have investigated the thermodynamics and the mass transfer kinetics of butyl benzoate on a monolithic and a packed RPLC column, with methanol–water (65:35, v/v) as the mobile phase. We showed that the BET isotherm model very accurately describes the adsorption behavior of this compound. The equilibrium-dispersive (ED) model and the lumped pore diffusion (POR) model were used to calculate the band profiles. An excellent agreement was obtained in this case between experimental and calculated band profiles but only because the value of the column efficiency N (with the ED model) or that of the overall mass transfer coefficient k_{ov} (with the POR model) were adjusted as functions of the concentration. The goal of this work is to investigate the mass transfer kinetics of butyl benzoate which has provided unusual and unexpected results in a prior comparative investigation of the thermodynamics of nonlinear equilibrium on conventional and monolithic columns [6,7].

To acquire relevant kinetics data, we measured the height equivalent to a theoretical plate (HETP) of small butyl benzoate peaks obtained by injecting small pulses on plateau concentrations of butyl benzoate, in a wide range of the methanol–water mobile phase velocity. The retention times and widths at half-height of these positive or negative perturbation peaks were determined [7]. We showed that to avoid ambiguity in establishing the value of molecular diffusivity a more sophisticated (GR) model should be used. The calculations showed that the GR model coupled with the modified BET isotherm and with an appropriate description of the variation of the internal porosity of the particles with the concentration of adsorbate affords an excellent approximation of the band profiles in the whole range of loading factors investigated.

2. Theory

2.1. General rate model

The GR model used in this work is similar to the GR model described in detail previously [12–14]. In order to apply this model, however, we need to determine the numerical values of the external mass transfer and the surface diffusion coefficients (see Section 4). We present here a short description of the GR model. In writing the equations of this model, we make the following assumptions:

1. The chromatographic process is isothermal.
2. The velocity of the mobile phase is constant. Its compressibility is negligible.
3. The solid matrix of a monolithic column consists of cylindrical tubes connected together [15–25]. We assume that the effective particle has a cylindrical shape.
4. The concentration gradient in the radial direction of the bed is negligible.
5. Local equilibrium exists for each component between the pore surface and the stagnant fluid phase in the macropores.
6. The dispersion coefficient is constant.
7. The external mass transfer resistance is ignored (see Section 4).
8. Surface diffusion can be ignored.
9. The internal porosity of the adsorbent depends on the adsorbate concentration.

With these assumptions, the differential mass balance for the species in the mobile phase can be expressed as follows:

$$\epsilon_e \cdot \frac{\partial C}{\partial t} + u \cdot \frac{\partial C}{\partial x} = \epsilon_e D_{\mathrm{L}} \cdot \frac{\partial^2 C}{\partial x^2} - (1-\epsilon_e) \cdot \frac{\partial \overline{C_p}}{\partial t} \qquad (1)$$

where:

$$\overline{C_{\mathrm{p}}} = \frac{2}{R_{\mathrm{p}}^2} \int_0^{R_{\mathrm{p}}} \epsilon_{\mathrm{p}} C_{\mathrm{p}} r \, \mathrm{d}r + \left(1-\epsilon_{\mathrm{p}}^0\right) \int_0^{R_{\mathrm{p}}} qr \, \mathrm{d}r \qquad (2)$$

The mass balance equation for the stagnant liquid phase within the pores of the particles can be written:

$$\frac{\partial\left[\epsilon_p(C_{\mathrm{p}})C_{\mathrm{p}}\right]}{\partial t} + \left(1-\epsilon_{\mathrm{p}}^0\right) c \frac{\partial q}{\partial t} = \frac{1}{r} \cdot \frac{1}{\partial r} \cdot \left[r \frac{D_{\mathrm{m}} \epsilon_{\mathrm{p}}(C_{\mathrm{p}})}{\theta(C_{\mathrm{p}})} \cdot \frac{\partial C_{\mathrm{p}}}{\partial r} \right] \qquad (3)$$

In Eqs. (1)–(3), C and C_p are the concentrations of the solute in the percolating stream and the stagnant liquid phase, respectively, q is the adsorbate con-

centration, x is the distance along the column, t is the time, r is the distance from the particle center, R_p is the particle diameter, ϵ_e is the external porosity, ϵ_p the internal or mesopore porosity (see Eq. (14)), ϵ_p^0 the initial value of the mesopore porosity (see Section 4.2.1), u is the superficial velocity, D_L (see Eq. (17)) is the axial dispersion coefficient, D_m is the molecular diffusivity (see Eqs. (19) and (21)), and θ is the pore tortuosity (see Eq. (15)).

In Eqs. (2) and (3) the concentration q is reported to the total adsorbent volume, i.e. to the sum of the volume of the solid skeleton of the particles and the volume of the pores inside these particle so, in the second term of the RHS of Eq. (2), the porosity is the initial mesopore porosity or value of the porosity when the solute concentration is equal to zero.

2.2. Isotherm model

The adsorption isotherm equation that best describes the adsorption isotherm data of butyl benzoate on the column used here is the Brunauer, Emmett, and Teller (BET) model [6]. This model is widely applied in gas–solid equilibrium [8–11]. The equation of this isotherm model extended to liquid–solid chromatography was derived and discussed previously [6]. It is written as:

$$q^* = \frac{H(C_p)}{[1 - b_L(C_p)][1 - b_L(C_p) + b_S(C_p)]} \tag{4}$$

where $H = b_S q_S$ is the Henry constant of adsorption, q_S is the monolayer saturation capacity of the adsorbent, b_S is the equilibrium constant for surface adsorption–desorption (on the free surface of the adsorbent) and b_L is the equilibrium constant for surface adsorption–desorption on a layer of adsorbate molecules.

2.3. Initial and boundary conditions

2.3.1. Initial condition

The model is completed by the following initial conditions:

For $t = 0$, the concentrations are:

$$C(0, x) = 0 \quad \text{for} \quad 0 < x < L \tag{5}$$

$$C_p(0, x, r) = 0 \quad q(0, x, r) = 0 \quad \text{for} \quad 0 < x < L \quad \text{and} \quad 0 < r < R_p \tag{6}$$

2.3.2. Boundary conditions for the first mass balance equation (Eq. (2))

These conditions are:

For $t > 0$ and at $x = 0$

$$u_f[C_f(t) - C(t, 0)] = -\epsilon_e D_L \cdot \frac{\partial C(0, t)}{\partial x} \tag{7}$$

with

$$C_f = 0 \quad \text{for} \quad t < 0 \quad \text{and} \quad \text{for} \quad t > t_p$$

and

$$C_f = C(t, 0) \quad \text{for} \quad 0 < t < t_p$$

For

$$t > 0 \quad \text{and} \quad \text{at} \quad x = L, \quad \frac{\partial C}{\partial x} = 0 \tag{8}$$

Eqs. (7) and (8) represent the classical Danckwerts boundary conditions.

2.3.3. Boundary conditions for the second mass balance equation (Eq. (4))

These conditions are:

For $t > 0, r = R_p$

$$C_p(t, r = R_p) = C \tag{9}$$

and for $t > 0, r = 0$

$$\frac{\partial C_p(t, r)}{\partial r} = 0 \tag{10}$$

2.3.4. Numerical solution of the general rate model

The GR model has no closed-form solutions. Numerical solutions were calculated using a computer program based on an implementation of the method of orthogonal collocation on finite elements [4,12,26,27]. The set of discredized ordinary differential equations was solved by the Adams–Moulton method, implemented in the VODE procedure [28]. The relative and absolute errors of the numerical calculations were $1 \cdot 10^{-6}$ and $1 \cdot 10^{-8}$, respectively.

3. Experimental

Complete details regarding the experimental work were previously published [7]. We report here only the most important experimental conditions.

3.1. Chemicals

The only mobile phase used in this work, whether for the determination of the adsorption isotherms data, for the elution of perturbation peaks, or for the acquisition of large size bands profiles was a mixture of HPLC-grade water and methanol (65% methanol, 35% water, v/v), both purchased from Fisher Scientific (Fair Lawn, NJ, USA). The solvents used to prepare the mobile phase were filtered before use on SFCA filter membrane, 0.2 μm pore size (Suwannee, GA, USA). Uracil and butyl benzoate were both obtained from Aldrich (Milwaukee, WI, USA).

3.2. Materials

A Chromolith Performance RP-18e, 100×4.6 mm, column was used. This C_{18}-bonded, endcapped monolithic column (column 22, Merck, Darmstadt, Germany) was one of six columns used previously by Kele and Guiochon in a study of the reproducibility of analytical data [29].

The hold-up time of this column was derived from the retention time of uracil. With the mobile phase composition used, the elution time of uracil is close to that of methanol or sodium nitrate [30] and gives an excellent estimate of the column void volume. The mean of at least five consecutive readings, agreeing to within 1%, was taken for each plateau concentration of the mobile phase [6]. The external porosity of the column was obtained from previously published results [6–31] ($\epsilon_e = 0.71$). The other physico-chemical properties of the column were supplied by the manufacturer [29] and are listed in Tables 1 and 3.

3.3. Apparatus

The data were acquired using a Hewlett-Packard (Palo Alto, CA, USA) HP 1090 liquid chromatograph. This instrument includes a multi-solvent delivery system (tank volume, 1 dm^3 each), an auto-sampler with a 25 mm^3 loop, a diode-array UV-detector, a column thermostat and a computer data acquisition station. Compressed nitrogen and helium bottles (National Welders, Charlotte, NC, USA) are connected to the instrument to enable the continuous operation of the pump and auto-sampler and the sparging of the eluent. The extra-column volumes are 0.056 and 0.340 cm^3 as measured by the auto-sampler and the pump system, respectively. All the retention data were corrected for this contribution. All measurements were carried out at the constant temperature of 23 °C.

Table 1
Physico-chemical properties of the monolithic silica columns supplied by the manufacturers [Merck]

Monolithic column (Merck)		Refs.
Skeleton size	1.3–1.5 μm	[29,34]
Macropore size	2 μm	
Mesopore size	130 Å	
Surface area (before C_{18} bonding)	300 m^2/g	
Surface coverage (C_{18})	3.6 μmol/m^2	
Total carbon	19.5%	
Endcapping	Yes	

3.4. Frontal analysis and isotherm measurements

Just prior any isotherm determination, a calibration curve was recorded for the solute at a wavelength of 293 nm. Thirty-seven data points were acquired, uniformly distributed within the concentration range investigated, from 0 to 10 g/dm^3. The calibration data are nonlinear and very well fitted to a third-degree polynomial.

A series of breakthrough curves are recorded successively at a flow-rate of 1 cm^3/min, with a sufficiently long time delay between each such curve to permit the reequilibration of the column with the pure mobile phase. The duration of sample injection depends on the time required for reaching the plateau concentration at the outlet of the column.

The retention volume of small pulses of uracil was determined from the average of five successive injections made at different plateau concentrations, from 0 to 12 g/dm^3, by step of 1.2 g/dm^3. The overloaded profiles needed for the validation of the fitted isotherms were recorded during the frontal analysis experiments.

3.5. Perturbation chromatography measurements

Van Deemter curves were measured with precision for various plateau concentrations of butyl benzoate. The mobile phase linear velocity u was increased step-wise. The flow-rate sequence (24 velocities) used for each plateau was as follows: 0.1→0.15→0.2→0.3→0.4→0.5→0.6→0.7→0.8→0.9→1.0→1.1→1.2→1.3→1.4→1.6→1.8→2.2→2.4→2.6→2.8→3.0→3.2 cm^3/min. Eight plateau concentrations were used, 0, 1, 2, 3, 4, 6, 8 and 10 g/dm^3. Negative then positive 25 mm^3 perturbations were injected for each determination. The negative pulse feed was prepared by dilution of the mobile phase used for the previous measurement. The positive pulse feed was prepared by adding a small amount of solute to the same volume of the current mobile phase. The exact concentrations of these pulses depended on the sensitivity of the detector, hence on the plateau concentration.

In order to obtain accurate results with the perturbation method, peaks with nearly Gaussian profiles should be obtained (which requires small perturbations) but these peaks must have the highest possible signal/noise ratio (which requires large peaks). The optimum wavelength, maximizing this ratio for a given perturbation, was 290 nm.

3.6. Overloaded chromatography peaks measurements

In order to validate the isotherm and the kinetic models derived here, series of profiles were acquired at a mobile phase velocity of 1.0 cm^3/min for loading factors between 0.1 and 15%.

4. Results and discussion

4.1. Estimation of the parameters of the kinetic model using the Van Deemter curves

The relationship between the HETP and the parameters of the thermodynamic and kinetic models was taken from the literature [2,3,13,14]:

$$H = \frac{L}{N_{GR}} = \frac{2D_L\epsilon_e}{u} + 2\frac{F\left[\epsilon_p + (1-\epsilon_p)\cdot\frac{dq}{dC}\right]}{1 + F\left[\epsilon_p + (1-\epsilon_p)\cdot\frac{dq}{dC}\right]} \cdot \left[\frac{d_p^2 u}{60FD_{eff}\epsilon_e} + \frac{d_p u}{6F\epsilon_e k_{ext}} + \left(\frac{k_p}{1+k_p}\right)^2 \cdot \frac{u}{F\epsilon_e k_a}\right] \quad (11)$$

where N_{GR} is the column efficiency derived from the GR model, $K \equiv b_s$ is the adsorption equilibrium constant, $F = (1-\epsilon_e)/\epsilon_e$, $k_p = FK$, and k_a is the adsorption rate constant. Assuming that the adsorption–desorption process itself is infinity fast and after substitution of D_L by the following expression [4,38]:

$$D_L = \gamma_1 D_m + \gamma_2 u d_p \quad (12)$$

we obtain:

$$H = \frac{2\gamma_1\epsilon_e D_m}{u} + 2\gamma_2\epsilon_e d_p + \left(\frac{k_1}{1+k_1}\right)^2 \cdot \left[\frac{d_p^2 u}{60F\epsilon_e D_{eff}} + \frac{d_p u}{6F\epsilon_e k_{ext}}\right] \quad (13)$$

where $k_1 = F[\epsilon_p + (1-\epsilon_p)\ dq/dC]$. This equation holds for spherical particles.

Miyabe and Guiochon have showed that in the case of cylindrical particles, the following expression holds [15]:

$$H = \frac{2\gamma_1\epsilon_e D_m}{u} + 2\gamma_2\epsilon_e d_p + \left(\frac{k_1}{1+k_1}\right)^2 \cdot \left[\frac{d_p^2 u}{32F\epsilon_e D_{eff}} + \frac{d_p u}{4F\epsilon_e k_{ext}}\right] \quad (14)$$

In order to use this equation, we need to determine the value of the following six parameters, γ_1, γ_2, D_m, D_{eff}, d_p, and k_{ext}. The simultaneous estimate of such a large number of parameters is difficult and can be only inaccurate. A brief example illustrates the difficulties encountered. It was not possible to fit the experimental data to Eq. (14) and derive best values of the six parameters. Numerical values were obtained only after coupling γ_1 D_m as one single parameter and assuming a value for k_{ext}. Then, it was

Table 2
Results of parameters estimated of Van Deemter curve

Parameter	Assumption 1		Assumption 2	Assumption 3
p1 = γ_2 (−)	0.818	K[p1, p2] = $3.238 \cdot 10^{-7}$ K[p1, p3] = −1	2.062	2.062
p2 = $\gamma_1 D_m$ (cm^2/s)	$1.326 \cdot 10^{-5}$	K[p1, p4] = −1 K[p2, p3] = $-3.277 \cdot 10^{-7}$	$1.326 \cdot 10^{-5}$	$1.326 \cdot 10^{-5}$
p3 = D_{eff} (cm^2/s)	$1.823 \cdot 10^{-6}$	K[p2, p4] = $-3.27 \cdot 10^{-7}$ K[p3, p4] = 1	$2.968 \cdot 10^{-7}$	$4.121 \cdot 10^{-7}$
p4 = d_p (cm)	$2.52 \cdot 10^{-4}$		$1 \cdot 10^{-4}$	$1 \cdot 10^{-4}$
p5 = k_{ext} (cm/s)	1000		1000	0.1

Italic = assumed parameters.

possible to estimate the values of the other parameters. Table 2 (under assumption 1) shows the correlation coefficients in the correlation matrix for the estimation of the four remaining parameters. The correlation coefficients between the parameters γ_2 and D_{eff} and between γ_2 and d_p are equal to −1. The correlation coefficient between the parameters D_{eff}, and d_p is equal to 1. These results do not make sense and confirm that it is impossible to determine the correct values of the model parameters.

Alternately, we may assume the value of one more parameter. Then, a three-parameter optimization gives the values listed in Table 2. The two parameters which are estimated approximately are the particle size and k_{ext} while the product $\gamma_1 D_m$ is considered as a single parameter. This leaves three other parameters for which the best calculated estimates are given in Table 2 with two assumed values for k_{ext}, 0.1 and 1000. In spite of this large difference, the best values for γ_2 and $\gamma_1 D_m$ are exactly the same and that for D_{eff} changes by a third. Using the set of values under assumption 2 (Table 2), we obtain a Van Deemter curve (solid line in Fig. 1) that is in excellent agreement with the experimental data (symbols). At this stage, given the precision of the experimental data and the various uncertainties affecting the theoretical model, it seems unrealistic to expect a better result.

4.2. Validation of the isotherm and kinetic models

4.2.1. Dependence of the total and internal porosities on the mobile phase concentration

The total porosity of the column used (column 22, Ref. [29]) was derived from the retention time of uracil, a non-retained compound. This retention time decreases with increasing butyl benzoate plateau concentration, by about 7% when the concentration increases from 0 to 12 g/dm^3. This decrease can be ascribed but to a similar decrease of the total column porosity ϵ_t. This decrease can be explained by the increasing volume of the adsorbate layer contained in the mesopores of the monolithic column.

The adsorption of butyl benzoate takes place essentially on the surface of the mesopores, inside the monolith skeleton, and changes in the total column porosity are due to changes in the mesopore or internal porosity. The macropore porosity is assumed to be constant in this work (ϵ_e = const).

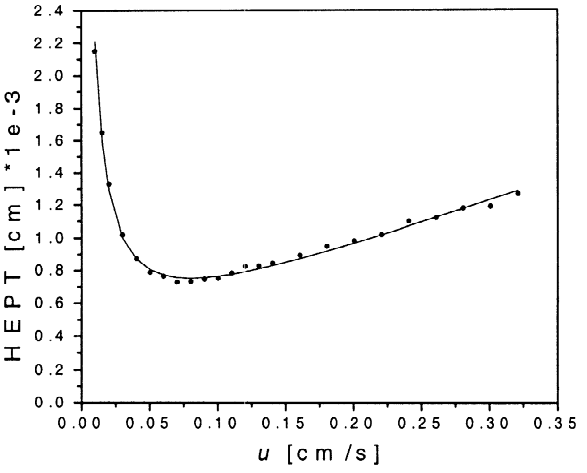

Fig. 1. Comparison between the experimental (symbols) HETP data derived from perturbation peaks injected on the lowest concentration plateau ($C = 0$ g/dm^3) and data calculated using the GR model and best estimates of the parameters (Table 2, assumption 2).

From the functional dependence of the total porosity on the butyl benzoate concentration in the mobile phase, the mesopore porosity is given by:

$$\epsilon_p(C_p) = \frac{\epsilon_t(C_p) - \epsilon_e}{1 - \epsilon_e} = \epsilon_p^0 - 0.0153C \quad (15)$$

In this equation, we approximated the experimental dependence of the internal porosity on the concentration using a linear function. The maximum changes of the porosity is about 40%. Fig. 2 compares the experimental data (symbols) and Eq. (15) (solid line). It should be emphasized at this stage that changes of the mesopore porosity cause changes in the mass transfer resistance inside the mesopores and also in the pore tortuosity parameter. These changes of ϵ_p are taken into account in the first and third term of Eq. (4). In the second term, however, we used the initial value of the mesopore porosity because the mass balance used for the determination of the isotherm model was referred to the volume of adsorbent in the column (see Eq. (16)).

Finally, we assumed that the pore tortuosity parameter can be expressed by the same equation as the one used in the cases when the particle porosity in independent of the solute concentration, so:

$$\theta = \frac{[2 - \epsilon_p(C)]^2}{\epsilon_p(C)} \quad (16)$$

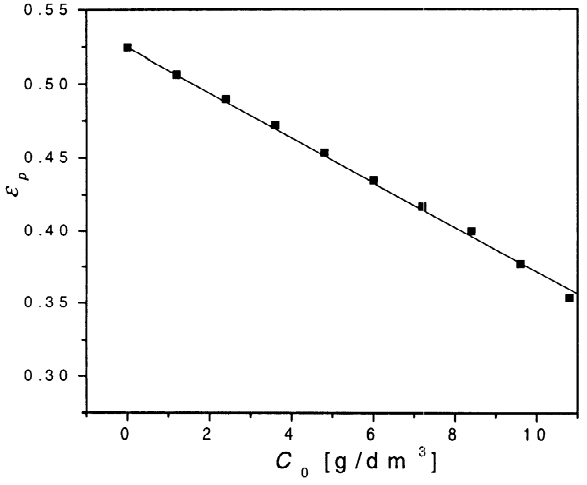

Fig. 2. Plot of the mesopore porosity of the monolithic column versus the concentration of butyl benzoate.

4.2.2. Discussion of isotherm model

In a previous report [6], we showed that the adsorption data measured for butyl benzoate on the monolithic column 23 ($\epsilon_t^0 = 0.841$), with methanol–water (65:35, v/v) as the mobile phase, fitted well to the liquid–solid extended BET isotherm model. The saturation capacity was $q_S = 209.2$ g/dm^3 and the surface equilibrium constants were $b_S = 0.120$ g/dm^3 and $b_L = 0.045$ g/dm^3. Thus the Henry constant was $H = q_S\ b_S = 25.10$.

In a following paper [7], the new isotherm parameters were derived from the following revised integral mass balance equation, in which the dependence of the column hold-up volume on the solute concentration was taken into account as:

$$q^* = \frac{C[V_{eq} - V_0 + V(C_p)]}{V_a} \quad (17)$$

where V_{eq} and V_0 are the elution volume of the equivalent area of the breakthrough curve and the hold-up volume, respectively, and V_a is the volume of stationary phase in the column. $V(C_p)$ is derived from the retention time of a nonretained compound at the plateau concentration, C_p.

The best values of the parameters of the isotherm model recalculated and estimated in this work from the breakthrough curves are reported in Table 3. The best estimate of the Henry constant is $H = 28.40$. These values differ from the former ones by less than 1.1%. The experimental isotherm data and the isotherm estimated from the model (solid line) are compared in Fig. 3. Although clearly visible, the upward curvature of the isotherm in the high concentration range is moderate. Less obvious is the downward curvature of the isotherm at low concentrations and the inflection point close to 2 mg/cm^3.

This behavior of the isotherm suggests that lateral interactions take place between adsorbed molecules. Among the many isotherm models investigated in an earlier study [6], models such as those of Fowler–Guggenheim and Jovanovic–Freundlich, which takes into account these lateral interactions, proved to be inadequate to account for the experimental data with the desired accuracy, compatible with the accuracy of the measured data. The best agreement between the experimental and theoretical isotherm data was afforded by a multi-layer adsorption model which is

Table 3
Values of the parameters used in the GR model

Parameter			Numerical value	
			Level "0"	Level "10"
Dispersion coefficient	D_L (cm^2/s)	(Eq. (17))	$2 \cdot 10^{-5}$	
Molecular diffusivity	D_m (cm^2/s)	(Eq. (19))	$2 \cdot 10^{-6}$	
Total porosity	ε_t^0		0.862	0.818
External porosity	ε_e		0.71	
Internal porosity	ε_p^0	(Eq. (14))	0.5255	0.3725
Tortuosity	θ^0	(Eq. (15))	4.137	7.111
Parameter of BET isotherm				
Monolayer saturation capacity	q_s (g/dm^3)		288.80	
Eq. const. for surface	b_S		0.09834	
Eq. const. for 2nd and *i*th layer	b_L		0.03962	

Level "0"—species plateau concentration $C=0$ [g/dm^3]; Level "10"—species plateau concentration $C=10$ [g/dm^3].

compatible with the well know BET isotherm for an infinite number of layers. The isotherm calculated from the BET model agrees well with the experimental data when assuming 13 layers [6].

The experimental isotherm was measured for butyl benzoate concentrations between $C=0$ and $C=10$ g/dm^3. For $C=10$ g/dm^3, the concentration of adsorbed butyl benzoate was $q=282$ g/dm^3. Taking into account the molecular mass (M=178), this gives values of 1.58 mol/dm^3, i.e. approximately 0.69 mmol/g or 2.2 mol/m^2. These calculations were performed assuming a density of silica equal

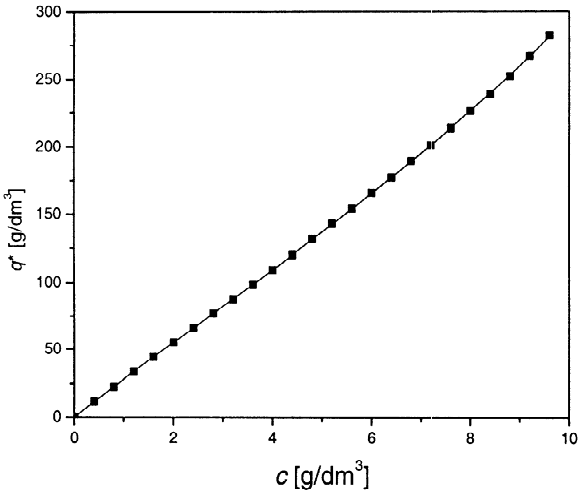

Fig. 3. Isotherm of butyl benzoate on the monolithic column, with methanol–water (65:35, v/v) as the mobile phase. $T=295$ K. The isotherm was calculated using Eq. (16).

2.3 g/cm^3 and a surface area of 300 m^2/g. The surface coverage of the octadecyl chains in the monolithic column is 3.6 mol/m^2. Accordingly, there are, on the average, about 6 molecules of butyl benzoate adsorbed for each 10 bonded alkyl chains.

Although these numerical results could be construed as consistent with the formation of a monolayer coverage of butyl benzoate on the octadecyl silica, the result of the simple calculation above is not compatible with the accurate modeling of the experimental data with the BET isotherm demonstrated previously [6]. This, however, does not preclude the possibility of the formation of local associations butyl benzoate molecules on some parts of the adsorbent pore structure. Despite the remaining uncertainty regarding the retention mechanism of butyl benzoate, we used the BET isotherm model in the following because the experimental data fits remarkably well to it.

4.2.3. Parameters of the GR model

In order to calculate band profiles as numerical solutions of the GR model, we need a number of parameters. To simplify these requirements, we made the following assumptions:

(i) The mass transfer resistance is negligible,

(ii) Eq. (12) is not used but D_L is calculated from the Gunn correlation (see Eq. (18)),

(iii) The effective diameter of the cylinders in the skeleton of the monolithic matrix of the column, d_p, was assigned an arbitrary value of 1.45 μm (Table

1). According to the manufacturer, this is the average skeleton size of the elements of the matrix structure of the monolithic columns [33]. This value is consistent with the various estimates available of the column permeability [15,29].

The axial dispersion coefficient in the mobile phase was calculated through Gunn equation [34], assuming that the variance distribution of the ratio between the fluid linear velocity and the average velocity over the column cross-section is zero. The Gunn equation is written:

$$\epsilon_e \cdot \frac{D_L}{d_p u} = \frac{ReSc}{4\alpha_1(1-\epsilon_e)} \cdot (1-p)^2 + \left[\frac{ReSc}{4\alpha_1(1-\epsilon_e)}\right]^2 \cdot p(1-p)^3 \cdot \left[e^{\frac{-4\alpha_1^2(1-\epsilon_e)}{p(1-p)ReSc}} - 1\right] + \frac{\epsilon_e}{\tau ReSc} \quad (18)$$

In this equation, α_1 is the first root of the zero Bessel function (2.40, 48); τ is the bed tortuosity factor, equal to 1.4 [34], and p is a parameter defined by [35]:

$$p = 0.17 + 0.33e^{-24/Re} \quad (19)$$

and $Re(=u\rho d_p/\eta)$ and $Sc(=\eta/\rho D_m)$ are the Reynolds and the Schmidt numbers, respectively, ρ is the density and η the viscosity of the mobile phase, respectively, and D_m is the molecular diffusivity of the solute in the mobile phase, approximated by the Wilke–Chang equation [36], extended to mixed solvents by Perkins and Geankoplis [37]:

$$D_m = 7.4 \cdot 10^{-8} \cdot \frac{T\sqrt{\phi M}}{\eta V_m^{0.6}} \quad (20)$$

where T is the absolute temperature, V_m is the molar volume of the solute at its normal boiling temperature, and ϕM is calculated from the mole fractions x_A and x_B of the two solvents and their association factors ϕ_A and ϕ_B:

$$\phi M = x_A \phi_A M_A + x_B \phi_B M_B \quad (21)$$

It must be noted that the Gunn equation was derived for bed of nonporous particles and that its applicability to monolithic columns has not been demonstrated yet.

The numerical values of the parameters used to calculate numerical solutions of the GR model and their dependence with the concentration between $C=0$ and $C=10$ g/dm^3 (highest plateau concentration of the solute) are listed in Table 3.

4.3. Validation of the GR model

To model the chromatography process when the internal or mesopore porosity depends strongly on the solute concentration, we propose the use of the GR model as described in Eqs. (2)–(4).

4.3.1. Molecular diffusivity D_m

To verify the validity of the model, we need the value of the molecular diffusivity, D_m. The value derived from the combination of Eqs. (20) and (21) is $4.5\cdot10^{-6}$ cm^2/s. However, solutions of the GR model calculated with this value have breakthrough fronts that are too steep. If we estimate the value of D_m by parameter identification, comparing experimental profiles and profiles calculated with different values of D_m, we obtain the markedly smaller value of $1.03\cdot10^{-6}$ cm^2. A comparison between an experimental breakthrough profile (symbols) and the calculated profile is shown in Fig. 4. The agreement is excellent.

Calculations were performed using the value of the effective monolith skeleton dimension indicated

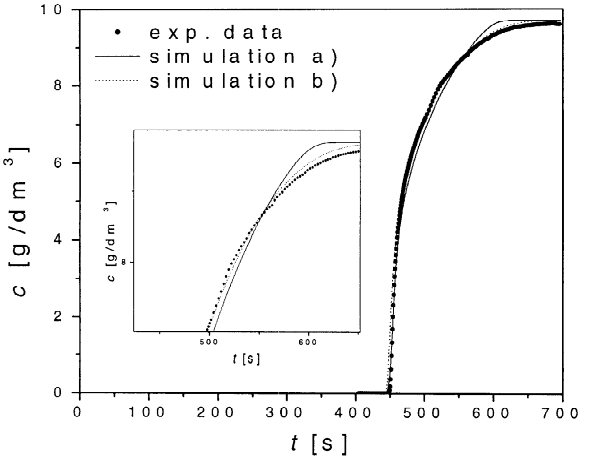

Fig. 4. Comparison of an experimental breakthrough curve (symbols) of butyl benzoate and the curves calculated using a values of the molecular diffusivity equal to: (a) $D_m=4.5\cdot10^{-6}$ cm^2/s; (b) $D_m=1.03\cdot10^{-6}$ cm^2/s.

earlier and the value of the molecular diffusivity D_m just estimated. The experimental peak profiles obtained for different values of the loading factor are compared with the results of these calculations in Fig. 5a–f. The agreement between the calculated and the experimental elution band profiles is generally excellent in the whole range of loading factors investigated, with $L_f = 0.7$ to 14%. However, all the experimental peak profiles exhibit a relatively long band tail which is not observed in calculated ones. This tailing results, at least in part, from the back-mixing that takes place in the solvent delivery system, probably in the pump [6]. Moreover, the experimental band profiles obtained at low values of the loading factor (for $L_f < 0.7$, e.g. see Fig. 5a and b) are shorter than the calculated ones because of this longer tail arising from the strongly disturbed injection profile that is not rectangular.

4.3.2. Validation using the Van Deemter data

We explained earlier that it was impossible to derive unambiguously the values of the model parameters from the experimental Van Deemter data. It is possible, however, to follow the converse approach and to compare these experimental data to those calculated using the GR model and the parameters estimated as explained earlier. This procedure would provide a measure of validation of the GR model.

Accordingly, we calculated with the GR model the profiles of linear, positive perturbations for a series of selected values of the mobile phase velocity and for each plateau concentration (see the values of these concentrations in Section 3.5). The values of the column HETP were derived from these profiles. The results of these calculations are compared to the experimental data in Fig. 6. There are clear differences between the two sets of values when the plateau concentration is between 0 and 3 g/dm^3 and in the range of linear velocity between 0.15 and 0.3 cm/s, i.e, under linear conditions and when the resistance to mass transfer of the solute between the stream of mobile phase and the stagnant mobile phase impregnating the solid-phase is dominant. In this range, the calculated perturbation peaks are shorter that the experimental ones and the difference between the height of the experimental and calculated peaks increases with increasing velocity. However, these differences decrease with increasing plateau concentration. At plateau concentrations between 6 and 10 g/dm^3, a range in which the phenomenon untypical running of the Van Deemter curves are observed [7], the difference between experimental and calculated data disappears. At a concentration of 10 g/dm^3 the agreement between the two sets of data is excellent. The result of this comparison confirms the validity of the GR model, particularly at high loadings of the column, when the pores of the stationary phase are largely filled with the adsorbate, i.e. for concentrations higher than 10 g/dm^3.

4.3.3. Application of the gr model to monolithic columns

Because it was not possible to determine independently accurate estimates of the different parameters of the GR model, it is impossible to use this model to ascertain the size of the structural elements of the monolithic column. Since the values of the parameters used in order to calculate the profiles shown in Fig. 5a–f were obtained by a procedure of parameter identification, it would be easy to obtain essentially the same band profiles for different values of the assumed apparent diameter of the cylinders of porous silica of the monolith by assuming appropriate values of the pore diffusivity.

We could as well assume that the monolithic matrix is made of spherical particles and then determine a value of the pore diffusivity for which the agreement between calculated and experimental band profiles would be the same as the one seen in Fig. 5a–f. Given the amount and nature of the experimental data available, it is not possible to determine unambiguously the shape of the structural elements in a column, the average size of these elements, nor the pore diffusivity.

5. Conclusion

The general rate model of chromatography can successfully predict chromatographic band profiles even when the mesopore volume changes because of the adsorption of feed components on the surface of the pores of the adsorbent. An excellent agreement is obtained between the experimental and the calculated

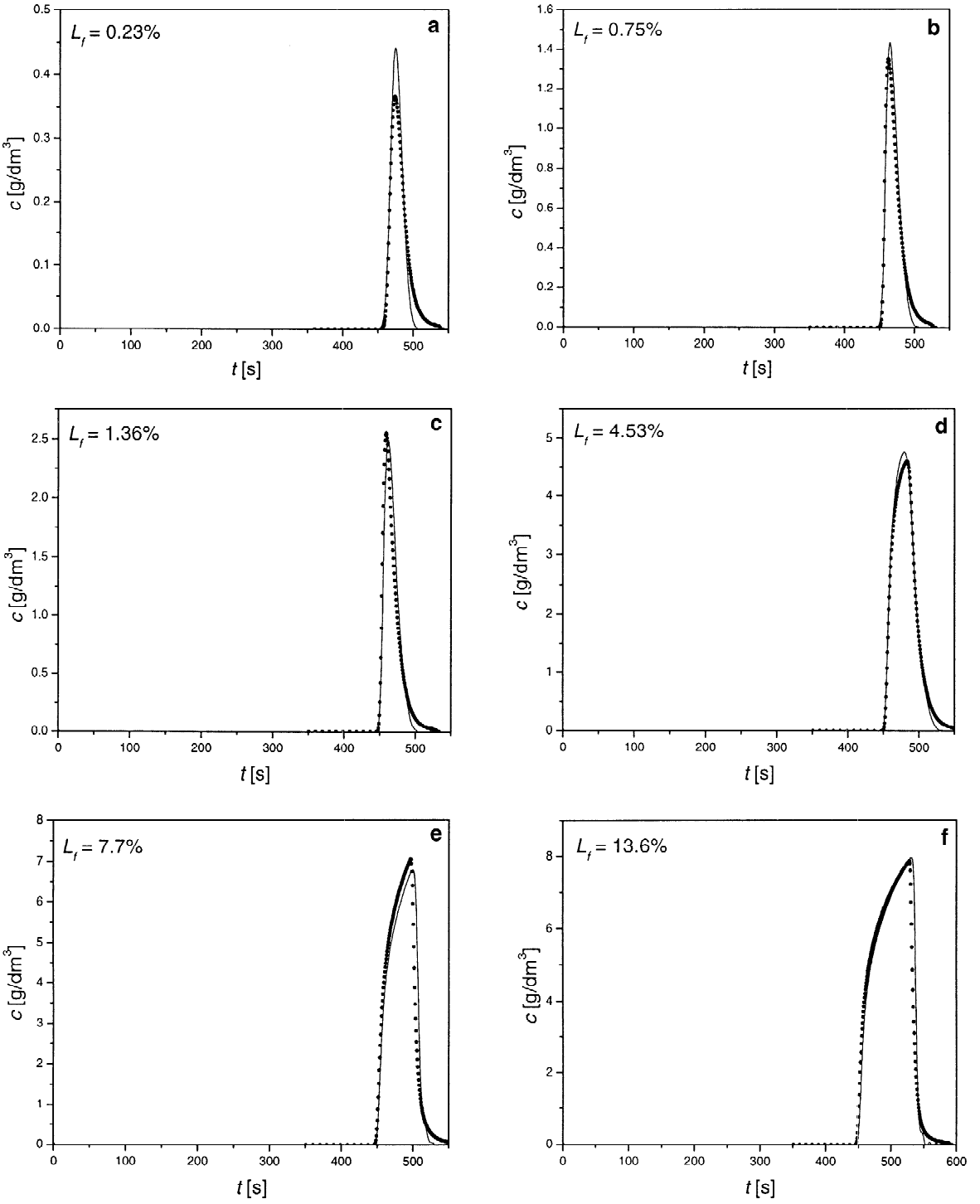

Fig. 5. Comparison of experimental (symbols) and calculated (solid lines) elution band profiles of butyl benzoate for different loading factors, L_f. Superficial velocity of the mobile phase $u = 0.1003$ cm/s.

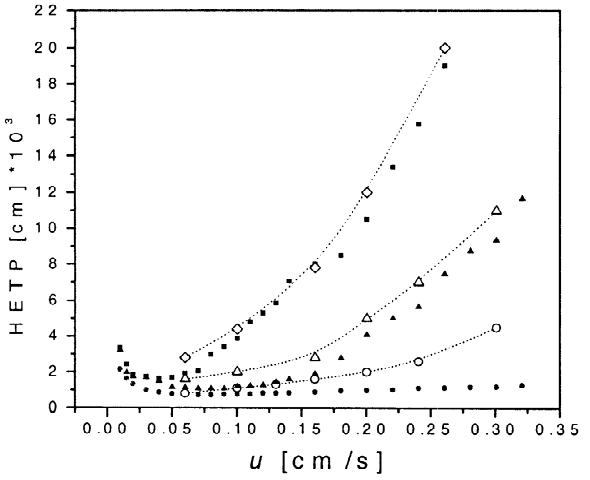

Fig. 6. Comparison between the HETP plots measured with the perturbation method and calculated with the GR model. Symbols: experimental data; solid lines: calculated curves. Plateau concentrations, $C = 0$ g/dm^3 (circle); $C = 6$ g/dm^3 (triangle); $C = 10$ g/dm^3 (square).

band profiles. The same excellent agreement was obtained in a wide range of loading factors, between 0.2 and 14%, while using the same value of the molecular diffusivity for all sample sizes. This contrasts with the situation observed with simpler models, such as the ED model, the lumped kinetic models, or the POR models for which it is often necessary to assume that the kinetic coefficient, e.g. the column efficiency N for the ED model, the lumped kinetic coefficient k_m, or the overall mass transfer coefficient k_{ov} for the POR model is a function of the concentration. This difference is ascribed to a model error, these simple models using only one or two kinetic parameters. The GR model presents also the interest that it can easily account for the dependence of the mesopore porosity on the concentration, something that the simpler models cannot do.

A full validation of the GR model would require, however, an independent estimate of the different kinetic parameters involved. Parameter identification affords the ability of making useful predictions and gives results that can be used for the optimization of the experimental conditions of a separation. As far the validation of the model is concerned, however, it would merely lead into a circular argument.

Acknowledgements

This work was supported in part by grant CHE-00-70548 from the National Science Foundation, by the cooperative agreement between the University of Tennessee and the Oak Ridge National Laboratory, and by grant 4T09C00623 of the Polish State Committee for Scientific Research.

References

[1] A.J. Berninger, R.D. Whitley, X. Zhang, N.-H.L. Wang, Comput. Chem. Eng. 15 (1991) 749.
[2] M. Suzuki, Adsorption Engineering, Elsevier, Amsterdam, 1990.
[3] D.M. Ruthven, Principles of Adsorption and Adsorption Process, Wiley, New York, 1984.
[4] G. Guiochon, S. Golshan-Shirazi, A.M. Katti, Fundamentals of Preparative and Nonlinear Chromatography, Academic Press, Boston, MA, 1994.
[5] V.J. Villadsen, M.L. Michelsen, Solution of Differential Equation Model by Polynomial Approximation, Prentice-Hall, Englewood Cliffs, NJ, 1978.
[6] F. Gritti, W. Piatkowski, G. Guiochon, J. Chromatogr. A 978 (2002) 81.
[7] F. Gritti, W. Piatkowski, G. Guiochon, J. Chromatogr. A (2003) in press.
[8] S. Brunauer, P.H. Emmet, E. Teller, J. Am. Chem. Soc. 60 (1938) 309.
[9] D.M. Young, A.D. Crowell, Physical Adsorption of Gases, Butterworths, London, 1962.
[10] L.E. Brecher, J.A. Kostecki, D.T. Camo, Phys. Adsorp. Proc. Principles 63 (1967) 18.
[11] L.E. Lecher, D.C. Frantz, J. A Kostecki, Phys. Adsorp. Proc. Principles 63 (1967) 25.
[12] K. Kaczmarski, A. Cavazzini, P. Szabelski, D. Zhou, X. Liu, G. Guiochon, J. Chromatogr. A 962 (2002) 57.
[13] K. Kaczmarski, D. Antos, J. Chromatogr. A 756 (1996) 73.
[14] K. Kaczmarski, D. Antos, H. Sajonz, P. Sajonz, G. Guiochon, J. Chromatogr. A 925 (2001) 1.
[15] K. Miyabe, G. Guiochon, J. Phys. Chem. B 106 (2002) 8898.
[16] H. Minakuchi, K. Nakanishi, N. Soga, N. Ishizuka, N. Tanaka, Anal. Chem. 68 (1996) 3498.
[17] H. Minakuchi, K. Nakanishi, N. Soga, N. Ishizuka, N. Tanaka, J. Chromatogr. A 762 (1997) 135.
[18] H. Minakuchi, K. Nakanishi, N. Soga, N. Ishizuka, N. Tanaka, J. Chromatogr. A 797 (1998) 121.
[19] N. Ishizuka, H. Minakuchi, K. Nakanishi, N. Soga, N. Tanaka, J. Chromatogr. A 797 (1998) 133.
[20] H. Minakuchi, K. Nakanishi, N. Soga, N. Ishizuka, N. Tanaka, J. Chromatogr. A 828 (1998) 83.
[21] N. Ishizuka, H. Minakuchi, K. Nakanishi, N. Soga, K. Hosoya, N. Tanaka, Anal. Chem. 72 (2000) 1275.

[22] K. Cabrera, D. Lubda, H.M. Eggenweiler, H. Minakuchi, K. Nakanishi, J. High Resolut. Chromatogr. 23 (2000) 93.
[23] K. Nakanishi, N. Soga, J. Am. Ceram. Soc. 74 (1991) 2518.
[24] K. Nakanishi, N. Soga, J. Non-Cryst. Solids 139 (1992) 1.
[25] K. Nakanishi, N. Soga, J. Non-Cryst. Solids 139 (1992) 14.
[26] K. Kaczmarski, G. Storti, M. Mazzotti, M. Morbidelli, Comput. Chem. Eng. 21 (1997) 641.
[27] J.A. Berninger, R.D. Whitley, X. Zhang, N.-H.L. Wang, Comput. Chem. Eng. 15 (1991) 749.
[28] P.N. Brown, A.C. Hindmarsh, G.D. Byrne, Variable Coefficient Ordinary Differential Equation Solver, 2000, Procedure available on http://www.netlib.org.
[29] M. Kele, G. Guiochon, J. Chromatogr. A 960 (2002) 19.
[30] K. Miyabe, G. Guiochon, Adv. Chromatogr. 40 (2000) 1.
[31] M. Al-Bokari, D. Cherrak, G. Guiochon, J. Chromatogr. A 975 (2002) 275.
[33] A. Cavazzini, G. Bardin, K. Kaczmarski, P. Szabelski, M. Al-Bokari, G. Guiochon, J. Chromatogr. A 925 (2001) 111.
[34] http://www.merck.de/english/services/chromatographie/hplc/chromolith/index.html
[35] D. Gunn, Chem. Eng. Sci. 42 (1987) 363.
[36] C.R. Wilke, P. Chang, AICHE J. 1 (1955) 264.
[37] L.R. Perkins, C.J. Geankoplis, Chem. Eng. Sci. 24 (1969) 1035.
[38] J.C. Giddings, United Separation Science, Wiley, New York, 1991.